Free-surface microfluidic control of surface-enhanced Raman spectroscopy for the optimized detection of airborne molecules

Brian D. Piorek*†, Seung Joon Lee‡, Juan G. Santiago§, Martin Moskovits‡, Sanjoy Banerjee*†, and Carl D. Meinhart†¶

Departments of *Chemical Engineering, †Mechanical Engineering, and ‡Chemistry and Biochemistry University of California, Santa Barbara, CA 93106; and §Department of Mechanical Engineering, Stanford University, Stanford, CA 94305

Communicated by Alan J. Heeger, University of California, Santa Barbara, CA, September 17, 2007 (received for review May 9, 2007)

We present a microfluidic technique for sensitive, real-time, optimized detection of airborne water-soluble molecules by surface-enhanced Raman spectroscopy (SERS). The method is based on a free-surface fluidic device in which a pressure-driven liquid microchannel flow is constrained by surface tension. A colloidal suspension of silver nanoparticles flowing through the microchannel that is open to the atmosphere absorbs gas-phase 4-aminobenzenethiol (4-ABT) from the surrounding environment. As surface ions adsorbed on the colloid nanoparticles are substituted by 4-ABT, the colloid aggregates, forming SERS ''hot spots'' whose concentrations vary predictably along the microchannel flow. 4-ABT confined in these hot spots produces SERS spectra of very great intensity. An aggregation model is used to account quantitatively for the extent of colloid aggregation as determined from the variation of the SERS intensity measured as a function of the streamwise position along the microchannel, which also corresponds to nanoparticle exposure time. This allows us simultaneously to monitor the nanoparticle aggregation process and to determine the location at which the SERS signal is optimized.

chemical detection | microfluidics | nanoparticle aggregation

An important trend in modern chemical reaction engineering is the miniaturization of reactors and other devices to the micro and nano scale (1). Such lab-on-a-chip systems, first postulated in 1990, and based on small-scale physics, now complement traditional reaction design approaches (2). In this work, we describe a microfluidic stream in which the spanwise dimension is miniaturized to a sufficiently small size to cause the flowing liquid to be confined solely by surface tension. This architecture allows a small-scale chemical processing device to be fabricated that allows gas-phase or airborne species to enter the flowing microfluidic circuit directly from the ambient environment. Once absorbed, these chemical species can potentially be subjected to further chemical reactions and analysis. Here, we demonstrate the absorption of a gas-phase species at a low partial pressure into a silver colloid flow confined to the microchannel and the subsequent detection of the analyte by surface-enhanced Raman spectroscopy (SERS). Because in this device reaction time scales proportionally with distance along the microchannel, this architecture allows the aggregation dynamics to be modeled and understood, making it possible to optimize the SERS signal intensity.

SERS spectra contain vibrational information that allows molecular species to be detected and identified (3, 4). First observed by Fleischmann and coworkers (5), and shown to be a highly enhanced form of Raman spectroscopy by Van Duyne (6), the SERS enhancement can be so great that analytes with femtomolar or lower concentrations can be detected (7), potentially making SERS a sensitive approach to detecting gaseous molecules emanating from explosive devices, toxic airborne compounds, or other atmospheric environmental contaminants (8).

The theory of SERS is now largely established. Most of the enhancement arises from the concentration of the electromagnetic optical fields near appropriately designed gold or silver nanosystems that are excited at or near surface-plasmon resonances (9). Some of the enhancement (referred to as chemical enhancement) arises from other optical resonances of the adsorbed molecule or the molecule–metal surface complex (10). It is now understood that the largest enhancements occur at ''hot spots'' (most commonly, nanosized gaps and interstices) where the electromagnetic optical field is especially concentrated (11). Under circumstances where there is a strong chemical enhancement acting in concert with the electromagnetic effect, Raman scattering can be enhanced by factors up to $\approx 10^{14}$. SERS enhancement factors in this regime enable fairly routine near-single-molecule detection sensitivity (12).

In this article, we report and analyze the time-dependent evolution of SERS ''hot particles'' (that is, of small aggregates that possess SERS hot spots) in a microchannel flow of Ag nanoparticles.

A free-surface flow through an open microchannel with a large surface-area-to-volume ratio, which we call free-surface fluidics, was used to control the exposure time of nanoparticles entrained in the flow to an analyte absorbed through the free surface (Fig. 1). This architecture acts as a SERS-based gas sensor in which the evolution of hot particles is controlled by the channel's microgeometry and the flow parameters. As a result, we are able to model and quantify the dynamics of aggregation and resulting Raman signal intensity.

The concentration of gas-phase molecules absorbed into the nanoparticle flow is related to the partial pressure of the gas-phase species above the free liquid surface by Henry's law. Once absorbed, the molecules drive nanoparticle aggregation kinetics according to the rate equation

$$k = k_0 e^{-V_0/(K_b T(1+\beta m)^{12/5})}, \qquad [1]$$

where k_o and V_o are constants, m is the concentration of analyte in solution, and β is a temperature-dependent constant (13). At constant temperature, the gas-phase partial pressure of the target molecules affects the rate of formation of SERS-active nanoparticle aggregates through its effect on m in Eq. **1**. When the concentration of the dissolved analyte is high, the nanoparticle aggregation rate approaches k_o independent of analyte concentration (13). Consequently, beyond a certain analyte

Author contributions: B.D.P., S.J.L., J.G.S., M.M., S.B., and C.D.M. designed research; B.D.P. and S.J.L. performed research; and B.D.P. wrote the paper.

The authors declare no conflict of interest.

Abbreviations: 4-ABT, 4-aminobenzenethiol; SERS, surface-enhanced Raman spectroscopy.

¶To whom correspondence should be addressed. E-mail: meinhart@engineering.ucsb.edu.

This article contains supporting information online at www.pnas.org/cgi/content/full/0708596104/DC1.

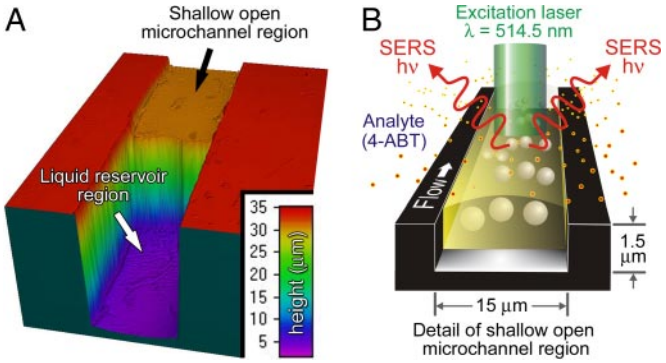

Fig. 1. Microfluidic/SERS sensing device. The device is designed for free-surface fluidics and is easily coupled with SERS detection. (*A*) Three-dimensional profile of the microfluidic device showing the transition from the 30-μm deep fluid reservoir to the open 1.5-μm-deep microchannel section. The flow channels are 15 μm wide and were characterized with 3D confocal microscopy (HS 200A Advanced Confocal Optical Profiler; Hyphenated Systems). (*B*) Schematic of microfluidic sensor for analysis of gas-phase species. The free-surface liquid/atmosphere interface allows analyte absorption and subsequent optical stimulation with a λ = 514.5 nm laser for SERS detection.

concentration and its corresponding gas-phase partial pressure, the observed maximum SERS intensity becomes more or less independent of the exposure time of the colloid to the analyte. At low values of m, however, the position of the SERS maximum in the microchannel will depend on m.

Results and Discussion

Three independent SERS intensity measurements were taken stepwise at 10-μm intervals between microchannel positions x_e = 0 μm and x_e = 570 μm. A typical series of SERS spectra, obtained by measuring the Raman scattering along the streamwise direction, x_e, of the microchannel in 10-μm increments, is shown in Fig. 2. The Raman spectrum shows only bands belonging to 4-aminobenzenethiol (4-ABT) (MW = 125 g/mol) (14); a negative control measurement of the system SERS response is shown in supporting information (SI) Fig. 5.

The SERS intensity of the 1,435-cm^{-1} Raman band of the 4-ABT is shown as a function of x_e in Fig. 3. The maximal SERS intensity occurs between distances of $x_e \sim 50$ μm to $x_e \sim 150$ μm. This corresponds to sol exposure times of $t_e \sim 1$ to $t_e \sim 3$ s assuming an average velocity of v_c = 60 μm/s.

In the streamwise direction of the flow, nanoparticle transport was dominated by convection since the associated Péclet number is $\mathrm{Pe}_L \equiv v_c L/D = 1 \times 10^3$, where v_c = 60 μm/s was the average flow velocity, L = 200 μm is a characteristic length scale in the streamwise direction of the microchannel flow, and $D = 1.13 \times 10^{-11}$ m^2/s is the nanoparticle diffusivity. The streamwise Péclet number also suggests that in the $x_e < 0$ region, thermal diffusion is insufficient to cause the sol to be exposed to the analyte. Because the system was designed such that chemical gradients in the depthwise direction of the flow would not affect aggregation dynamics, the nanoparticle distribution was nearly constant in the depthwise direction, h, of the microchannel flow. The ratio of the diffusion time scale in the depthwise direction to the advection time scale is $(v_c L/D)\cdot(h/L)^2 = 3 \times 10^{-2}$, where h = 1 μm is a characteristic length scale in the depthwise direction. In addition, the 4-ABT concentration was nearly constant in the depthwise direction of the microchannel flow since $(v_c L/D)\cdot(h/L)^2 = 3 \times 10^{-3}$, where $D = 1 \times 10^{-10}$ m^2/s is the diffusivity of 4-ABT (15).

The 1.5-μm-deep microchannel interrogation region is matched to the penetration depth of the SERS excitation laser and the Raman signal collection optics. The confinement of analyte and SERS-active species to the laser penetration depth eliminates signal losses due to diffusion away from the SERS interrogation system.

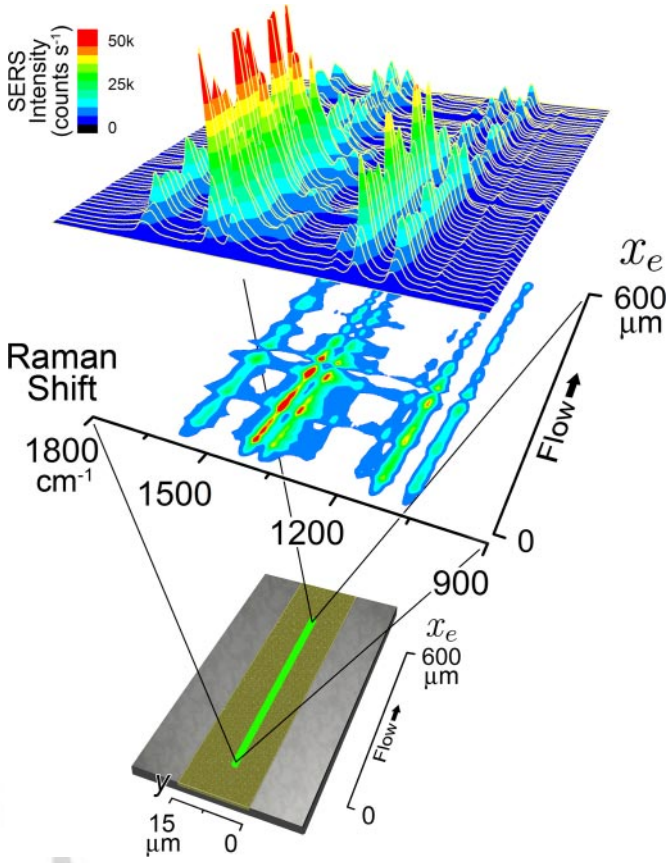

Fig. 2. Typical series of SERS spectra, obtained by the stepwise measurement of Raman scattering along the microchannel in 10-μm increments, shown as a function of position down the streamwise direction of the microchannel. The SERS interrogation path down the central region of the microchannel is shown (straight green line).

The sensor signal diminishes in the 30-μm-deep downstream fluid reservoir at values of $x_e > 530$ μm. In this region, the 20-fold increase in depth allows the SERS-active species to diffuse away from the SERS laser penetration region, resulting in the detection of fewer nanoparticle clusters.

The 4-ABT analyte molecules (calculated by using ACD/Labs V.8.14 for Solaris; Advanced Chemistry Development) and the Ag nanoparticles are soluble and are readily absorbed by the aqueous medium. We assume that the Ag nanoparticle aggregation dynamics are not affected by capillary forces at the gas–liquid interface because the suspended Ag nanoparticles are hydrophilic and homogeneously distributed in the liquid volume (16). We also assume that the aggregation of three or more nanoparticles is limited by the reduced diffusivity of these larger clusters (17, 18).

The shape of the SERS intensity versus flow-time curve shown in Fig. 3 is readily explained in terms of nanoparticle aggregation kinetics. The nanoparticle aggregation process is shown schematically in Fig. 4. The nanoparticles are originally in free suspension (Fig. 4*A*). When 4-ABT is introduced into the flowing solution through the free-surface interface, 4-ABT binds to the nanoparticles, initiating the aggregation process. Monomers (Fig. 4*B*) form dimers (Fig. 4*C*), which, in turn, form trimers (Fig. 4*D*), and so on. Ag particle-adsorbate dimers (Fig. 4*C*) are ≈3–4 orders of magnitude more SERS-active than

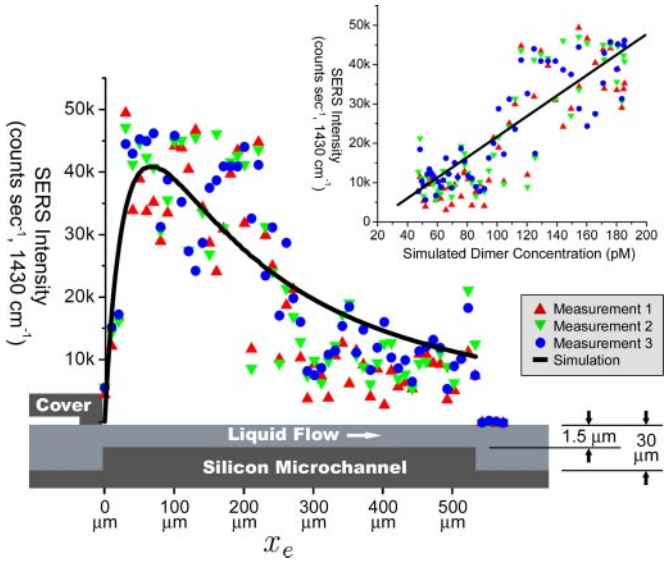

Fig. 3. Measured SERS intensity shown above a diagrammatic side view of the microchannel (triangles, inverted triangles, and circles). The simulated aggregation profile (solid line) assumes that SERS intensity is due exclusively to nanoparticle dimers. (*Inset*) Measured SERS intensity shown as a function of simulated dimer concentration.

monomers (Fig. 4*B*) (11). Likewise, the SERS responses of aggregate assemblies of more than two nanoparticles (e.g., trimers; Fig. 4*D*) normally have SERS cross-sections that are somewhat smaller (on a per-adsorbed-molecule basis) than that of the dimers (19). We therefore assume that the SERS intensity is dominated by and therefore approximately proportional to nanoparticle dimer concentration.

The free-surface colloid aggregation process was simulated by using COMSOL Multiphysics V.3.3 (COMSOL). Diffusion constants for one- to four-nanoparticle aggregates were calculated from the Stokes–Einstein equation by using the geometric mean aggregate diameter. Because the diffusivity decreases for increasing aggregate size, the nanoparticle aggregation rates decrease with increased aggregate size.

The convection and diffusion equation for nanoparticle aggregate concentration

$$\frac{\partial C_i}{\partial t} + (u\cdot\nabla)C_i = \nabla\cdot(D_i\nabla C_i) + R_i \qquad [2]$$

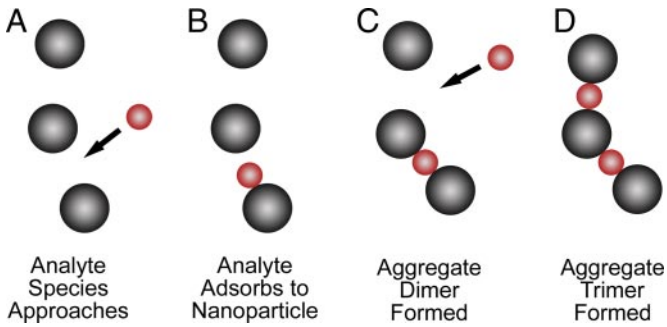

Fig. 4. Schematic formation of nanoparticle aggregates by the stepwise addition of adsorbate molecules (red spheres). (*A*) Initial unbound state of the nanoparticles. (*B*) A single nanoparticle is bound to an adsorbate molecule, forming a monomer. (*C*) Two nanoparticles are bound to a single adsorbate molecule, forming a dimer. (*D*) Three nanoparticles are bound to two adsorbate molecules, forming a trimer.

was solved in 2D space according to the reaction equations

$$\begin{aligned} R_1 &= -2k(C_1C_1) - k(C_2C_1) - k(C_3C_1) \\ R_2 &= k(C_1C_1) - k(C_2C_1) - 2k(C_2C_2) \\ R_3 &= k(C_2C_1) - k(C_3C_1) \\ R_4 &= k(C_3C_1) + k(C_2C_2), \end{aligned} \qquad [3]$$

where C_1 is the concentration of unbound nanoparticles (Fig. 4*A*), C_2 is the concentration of nanoparticle dimers (Fig. 4*C*), C_3 is the concentration of nanoparticle trimers (Fig. 4*D*), C_4 is the concentration of nanoparticle tetramers, and D_i is the respective nanoparticle-aggregate diffusivity. The Navier–Stokes and conservation of mass equations were used to find the flow velocity $\boldsymbol{u}$, and k is the nanoparticle aggregation rate constant of Eq. **1**. The rate of 4-ABT adsorption to the Ag nanoparticles was assumed to dominate the analyte-particle desorption coefficient as previously shown by experimental and molecular dynamics simulation results (20). The value $k = 10^6$ m^3/mol^{-2} was chosen because it compares well with the experimental SERS intensity data shown in Fig. 3.

The simulation model accurately preserves the mobility ratio of the lower-order aggregate species and omits the contributions of larger aggregates that, at any rate, contribute less efficiently to Raman scattering. The solution to this system is shown in Fig. 3 (solid line). The correspondence between the calculated and observed SERS intensity profile as a function of streamwise position falls within the scatter of the experimental data.

The SERS cross-section of the 4-ABT molecules—that is, the ratio of SERS response per 4-ABT molecule in solution—was estimated by assuming that one analyte molecule was present and reporting the SERS response per nanoparticle dimer. Comparing the measured SERS response with the simulated concentration of nanoparticle dimers along the microchannel (Fig. 3 *Inset*) produces a proportional relationship (with a correlation coefficient of $R^2 = 0.78$). This suggests that the SERS cross-section is approximately constant along the entire length of the microchannel: before, at, and subsequent to the SERS maximum. In view of this, the assumption that it is the nanoparticle dimers that provide the majority of SERS response appears to be a reasonable one.

The maximum simulated concentration of nanoparticle dimers is 190 pM. This concentration indicates that, on average, approximately six dimers were interrogated during the 1-s Raman signal accumulation period in the $\approx$1.2-μm^3 focal volume. The scatter in the observed SERS intensity reported in Fig. 3 is, therefore, not noise but a function of the small-number statistics of the particles crossing into the laser beam.

One should bear in mind that the sensor we describe works only with water-soluble analytes that also induce nanoparticle aggregation. Aggregation might occur either as a result of the nanoparticle-linking capabilities of the analyte through intrinsic functionalities such as thiolate or amine groups or through its ability to reduce the Coulomb barrier to colloid aggregation, as was the case in this study. Although this restriction means that the sensor will not be responsive to some analytes, the range of molecules for which it will be sensitive is very large and embraces many classes of compounds (most explosives, for example) for which better sensing methods are still active research and development goals. Accordingly, despite the limitation to water-soluble analytes, this is potentially a valuable and broadly applicable approach.

Although we do not envision the sensor to be a competitor to microfluidic flow tracing techniques such as microPIV (21), the system might be used to monitor reaction intermediates or products in reacting flows, either as two converging microfluidic

liquid streams or in a liquid sensor channel that monitors the intermediates or products of a nearby gas-phase reaction.

Conclusions

A free-surface microfluidic device is described for continuous analysis of airborne molecules. Surface tension at the free-surface interface is used to confine the pressure-driven flow at rate of 60 μm/s through the 1.5 μm $\times$ 15 μm microchannel. The free surface allows airborne species to be absorbed directly into the fluid flowing in the microchannel. SERS was used to detect the presence of gaseous 4-ABT molecules that became entrained into the liquid phase.

The SERS intensity was measured as a function of streamwise position in the microchannel. Its intensity indicated the formation of SERS hot molecules resulting from adsorbate-mediated nanoparticle aggregation. The 10^{-9} M Ag colloid solution required exposure times of $\approx$1 to $\approx$3 s to generate maximal SERS intensities when exposed to gaseous $\approx$300 μM 4-ABT. Numerical simulation of sol aggregation dynamics confirmed the time-dependent formation and depletion of dimers in the microchannel flow and accounted for the observed position of the SERS intensity maximum.

This system is the basis of a sensitive, microfluidics-based sensor for real-time, continuous monitoring of water-soluble gas-phase or airborne agents. It also allows one to optimize the SERS measurements by choosing the position along the channel where the dimer concentration is maximum. In its current embodiment, the sensor will only detect an analyte that is at least somewhat water soluble. However, a device capable of overcoming this limitation that nevertheless incorporates the fundamental idea of this sensor can be designed. For example, one can bring together two (or multiple) parallel streams, with aqueous and nonaqueous liquids flowing through them, with the analyte dissolved in an appropriate solvent and transferred onto the nanoparticles at the interface between two streams.

Materials and Methods

The dynamics and performance of the free-surface fluidic device were investigated by absorbing vapor-phase 4-ABT molecules into a microchannel flow of a solution of 35–40 nm diameter Ag nanoparticles. Once absorbed into the flowing nanoparticle solution, the 4-ABT molecules diffuse to, and adsorb onto, the nanoparticle surfaces, displacing charged adsorbed species from the nanoparticles' surfaces and encouraging the nanoparticles to aggregate, resulting in the formation of SERS hot particles. (It is charged particles adsorbed on the colloidal particles' surfaces that stabilize them by Coulomb repulsion.) By following the development of the SERS spectrum, one can simultaneously follow the step-by-step nanoparticle aggregation process and determine the identity and (under appropriate circumstances) partial pressure of the gas-phase analyte even at low partial pressures.

The device design is shown schematically in Fig. 1*A*. A Ag sol is pumped through an enclosed 30-μm-deep by 15-μm-wide fluid reservoir into a shallow microchannel that is 1.5 μm deep by 15 μm wide. The relatively large depth of the fluid reservoir (30 μm) reduces contamination upstream of the microchannel, allowing temporally resolved exposure measurements to be carried out. The resulting velocity is 60 μm/s (22). The Ag sol consists of 35- to 40-nm-diameter Ag nanoparticles at a concentration of 10^{-9} M. The constant velocity in the channel is driven by surface tension forces at end-channel reservoirs. (Details of the preparation of the nanoparticle solution are given in *SI Text*.)

A PID temperature controller was used to maintain the sol temperature at the dew point to minimize evaporative solvent loss at the free surface. Raman measurements were carried out at various spots along the channel. The 1.5-μm-deep microchannel drains into a 30-μm-deep by 15-μm-wide enclosed fluid reservoir. The Laplace pressure at the free-surface interface is controlled throughout the microchannel system by judiciously choosing the volume of the fluid reservoirs. The resulting pressure gradient drives the free-surface flow and allows the microchannel flow velocity to be precisely controlled.

Gas-phase sensing performance was demonstrated by establishing a low partial pressure of 4-ABT in the vicinity of the microchannel at room temperature. A small pellet of 4-ABT and the microchannel were housed within a sealed box (10 cm diameter by 0.6 cm height). The solid sample was placed $\approx$3 cm from the open sol flow and allowed to equilibrate for 15 min before SERS measurements were performed. The gas-phase concentration of 4-ABT in the containment box was estimated to be $\approx$300 μM.

A focused λ = 514.5 nm laser (Spectra-Physics 164; continuous wave) beam ($\approx$1 μm diameter) was used as the Raman excitation source. The laser was scanned in the streamwise direction at 10-μm steps along the midline of the 1.5-μm-deep open microchannel. Scattered light was collected with a $\times$50 objective and analyzed with a confocal Raman spectroscopy system (LabRAM microRaman system; Jobin-Yvon; equipped with a thermoelectrically cooled CCD detector). Each spectrum was collected in 1 s with 50 mW of laser power. The exposure time of the sol to the vapor, t_e, is given approximately by $t_e = x_e/v_c$ where x_e is the streamwise sol travel distance during exposure and v_c is the liquid velocity near the free surface. At constant flow, the distance from $x_e = 0$ to the interrogation position along the channel is approximately proportional to the substrate exposure time to the analyte. This allows the SERS signal from SERS-active nanoparticle aggregates to be continuously monitored as it evolves after exposure to the analyte.

We thank John Tamelier for helpful microfabrication assistance and two anonymous reviewers for their comments. This work was supported by U.S. Army Research Office/Institute for Collaborative Biotechnologies Grant DAAD19-03-D-0004, Air Force Office of Scientific Research Grant FA9950-04-0106, and National Science Foundation/Nanoscale Interdisciplinary Research Teams Grant CTS-0404444.

1. Hu X, Bessette PH, Qian J, Meinhart CD, Daugherty PS, Soh HT (2005) *Proc Natl Acad Sci USA* 102:15757–15761.
2. Manz A, Graber N, Widmer HM (1990) *Sens Actuators B* 1:244–248.
3. Zhang X, Young MA, Lyandres O, Van Duyne RP (2005) *J Am Chem Soc* 127:4484–4489.
4. Cao YC, Jin R, Mirkin CA (2002) *Science* 297:1536–1540.
5. Fleischmann M, Hendra PJ, McQuillan AJ (1974) *Chem Phys Lett* 26:163–166.
6. Jeanmaire DL, Van Duyne RP (1977) *J Electroanal Chem* 84:1–20.
7. Grubisha DS, Lipert RJ, Park H-Y, Driskell J, Porter MD (2003) *Anal Chem* 75:5936–5943.
8. Dubnikova F, Kosloff R, Almog J, Zeiri Y, Boese R, Itzhaky H, Alt A, Keinan E (2005) *J Am Chem Soc* 127:1146–1159.
9. Moskovits M (1985) *Rev Mod Phys* 57:783–826.
10. Otto A, Mrozek I, Grabhorn H, Akemann W (1992) *J Phys Condens Matter* 4:1143–1212.
11. Xu H, Bjerneld EJ, Käll M, Börjesson L (1999) *Phys Rev Lett* 83:4357–4360.
12. Kneipp K, Wang Y, Kneipp H, Perelman LT, Itzkan I, Dasari RR, Feld MS (1997) *Phys Rev Lett* 78:1667–1670.
13. Moskovits M, Vlckova B (2005) *J Phys Chem B* 109:14755–14758.
14. Schierhorn M, Lee SJ, Boettcher SW, Stucky GD, Moskovits M (2006) *Adv Mater* 18:2829–2832.
15. Wilke CR, Chang P (1955) *AIChE J* 1:264–270.
16. Vincze A, Agod A, Kertesz J, Zrinyi M, Horvolgyi Z (2001) *J Chem Phys* 114:520–529.
17. Witten TA, Sander LM (1981) *Phys Rev Lett* 47:1400–1403.
18. Jullien R, Kolb M, Botet R (1984) *J Phys (Paris)* 45:395–399.
19. Moskovits M (2005) *J Raman Spectrosc* 36:485–496.
20. Meyer M, LeRu EC, Etchegoin PG (2006) *J Phys Chem B* 110:6040–6047.
21. Meinhart CD, Wereley ST, Santiago JG (1999) *Exp Fluids* 27:414–419.
22. Piorek B, Mechler A, Lal R, Freudenthal P, Meinhart C, Banerjee S (2006) *Appl Phys Lett* 89:153123.